Passive Ballistic Microbunching of Nonultrarelativistic Electron Bunches Using Electromagnetic Wakefields in Dielectric-Lined Waveguides

F. Lemery,[1,*] P. Piot,[2,3] G. Amatuni,[4,5] P. Boonpornprasert,[4] Y. Chen,[4] J. Good,[4] B. Grigoryan,[4,5] M. Groß,[4] M. Krasilinikov,[4] O. Lishilin,[4] G. Loisch,[4] A. Oppelt,[4] S. Philipp,[4] H. Qian,[4] Y. Renier,[4] F. Stephan,[4] and I. Zagorodnov[1]

[1]*Deutsches Elektronen-Synchrotron, Notkestraße 85, 22607 Hamburg, Germany*
[2]*Northern Illinois Center for Accelerator & Detector Development and Department of Physics, Northern Illinois University, DeKalb Illinois 60115, USA*
[3]*Accelerator Physics Center, Fermi National Accelerator Laboratory, Batavia, Illinois 60510, USA*
[4]*Deutsches Elektronen-Synchrotron, Platannenallee 6, 15738 Zeuthen, Germany*
[5]*Center for the Advancement of Natural Discoveries using Light Emission, Yerevan 0040, Armenia*

Temporally modulated electron beams have a wide array of applications ranging from the generation of coherently enhanced electromagnetic radiation to the resonant excitation of electromagnetic wakefields in advanced-accelerator concepts. Likewise producing low-energy ultrashort microbunches could be useful for ultrafast electron diffraction and new accelerator-based light-source concepts. In this Letter we propose and experimentally demonstrate a passive microbunching technique capable of forming a picosecond bunch train at ∼6 MeV. The method relies on the excitation of electromagnetic wakefields as the beam propagates through a dielectric-lined waveguide. Owing to the nonultrarelativistic nature of the beam, the induced energy modulation eventually converts into a density modulation as the beam travels in a following free-space drift. The modulated beam is further accelerated to ∼20 MeV while preserving the imparted density modulation.

Forefront applications of electron beams call for increasingly precise spatiotemporal control over the beam phase-space distribution. Beam-manipulation techniques to tailor electron bunch distributions have flourished over the last decade and include various degrees of complexity [1–5]. Recently, methods to passively shape the temporal (or current) distribution of an electron beam have emerged [6–9]. In essence, this class of techniques uses a dielectric-lined waveguide (DLW) to impart an arbitrary time-energy correlation along an electron bunch; subsequently a suitable beam line converts the induced energy correlations into the desired current profile. The techniques successfully demonstrated so far [6,8] were realized at relativistic energies and use a dispersive section composed of a magnetic chicane [10] to manipulate the current profile. Likewise the Čerenkov free-electron laser (FEL) relies on a microbunching instability developed by a self-interaction via a radiative field [11–13].

In this Letter we demonstrate that a DLW located directly downstream of a photoemission electron source supports the formation of a current-modulated beam over a drift in free space. In our experiment the technique realizes mm-scale modulation wavelengths for a high-charge (1 nC) electron bunch. Compared to Ref. [6], which produced a mm-scale modulation using a 70-MeV bunch, our scheme avoids the use of a magnetic-based dispersive section with

its associated phase-space dilution in the bending-plane degree of freedom [14]. It should be stressed that the observed beam modulation within picosecond-scale bunches over short interaction distances (<10 cm) and does not rely on the Čerenkov-FEL process explored in Ref. [13]. Additionally, the formed current-modulated beams could be injected in a subsequent linear accelerator for further tailoring and usage. The availability of shaped low-energy modulated beams [15] could have direct application to THz light sources [16,17], ultrafast electron diffraction (UED) [18–20], and serve as injectors for, e.g., beam-driven advanced-accelerator concepts [21].

In order to quantify the proposed self-bunching mechanism, we model the electron bunch as a line-charge distribution and analyze the dynamics of the electrons in the longitudinal phase space (LPS) with coordinates (ζ, δ) where ζ refers to the axial position of an electron with respect to the bunch's center and $\delta \equiv p/\langle p \rangle - 1 \simeq \Delta p_z/\langle p_z \rangle$ is the fractional momentum offset of an electron; here $\langle p \rangle$ represents the bunch mean momentum (p_z refers to the longitudinal momentum). The axial field associated to the wakefield generated by the electron bunch is given by $E_z(\zeta) = \int_{-\infty}^{\zeta} \Lambda(\zeta - \zeta') \sum_{n,m} w_n^{(m)} \cos(k_n^{(m)} \zeta') d\zeta'$, where the double sum is evaluated on the number of modes $n = 1$, N categorized as monopole ($m = 0$) and dipole ($m = 1$)

modes supported by the DLW. The parameters $w_n^{(m)}$ and $k_n^{(m)}$ are, respectively, the field amplitude and wave vector associated to the mode (n, m), and $\Lambda(\zeta) \equiv \int_{-\infty}^{+\infty} d\delta \Phi(\zeta, \delta)$ [here $\Phi(\zeta, \delta)$ is the LPS density distribution] is the charge density with the total bunch charge given by $Q = \int_{-\infty}^{+\infty} d\zeta \Lambda(\zeta)$. For simplicity we only consider the dominant monopole ($m = 0$) mode $n = 1$ and introduce $w \equiv w_1^{(0)}$ and $k \equiv k_1^{(0)}$. As an example we consider the case of a semi-Gaussian distribution $\Lambda(\zeta) = (Q/\sqrt{2\pi\sigma^2}\mathcal{N})$ $\{\exp[-(\zeta - \mu)^2/2\sigma^2]\Theta(\zeta - \mu) + \Theta[-\zeta + \mu]\}$, where μ and $\sigma > 0$ are, respectively, the rising edge center and rms width, $\mathcal{N} > 0$ is a normalization constant, and $\Theta()$ the Heaviside function. Upon satisfying the transcendental condition $\lambda = (4\pi\sigma/\sqrt{2})D(\sqrt{2\pi}\sigma/\lambda)$ (with solution $\sigma \simeq 5\lambda$), where $D()$ is the Dawson function [22] and $\lambda \equiv 2\pi/k$ is the mode wavelength, the wakefield reduces to $E_z(\zeta) = (Q/\mathcal{N})\exp[-(2\pi^2\sigma^2N/\lambda^2)]\cos[k(\zeta - \mu)]$. Hence an initially smooth LPS distribution in (ζ_0, δ_0) [Fig. 1(b)] is energy modulated as it interacts with its wakefield over the length l following $\delta_0 \to \delta_d = \delta_0(\zeta_0) + eV/(\gamma_0 mc^2)$ $\cos(k\zeta_0 + \psi)$, where γ_0 is the Lorentz factor, ψ an arbitrary phase and V the modulation potential (for the distribution above $V \equiv Ql/\mathcal{N}$ and $\psi \equiv -k\mu$); see Fig. 1(c). The beam transport through the downstream drift space can be described by the linear transformation $\zeta_0 \to \zeta_f = \zeta_0 + \xi\delta_d$, where $\xi \simeq -L/\gamma_f^2$ is the longitudinal dispersion of a drift space with length L, and γ_f is the Lorentz factor downstream of the DLW structure. A proper choice of L and γ_f leads to the energy modulation being converted into a density modulation at a given location downstream [7] and the density modulation period is equal to the mode wavelength $\Delta\zeta \simeq \lambda$; see Fig. 1(d).

The experiment was performed at the photoinjector test facility at DESY in Zeuthen (PITZ) [23] diagrammed in Fig. 1(a). In brief, the $\sim$6.2 MeV/c electron bunches are generated in an L band ($f = 1.3$ GHz) radio frequency (rf) photoemission electron source and directly focused into a DLW and further transported in a drift space up to a linear accelerator (linac) for acceleration to a final momentum of $\sim$20 MeV/c [24]. The rf gun comprises a cesium telluride photocathode illuminated by an ultraviolet laser pulse with a super-Gaussian temporal distribution produced via coherent pulse stacking using a Šolc filter [25]. The DLW is located $z_c = 1.71$ m from the photocathode and the solenoidal lenses surrounding the gun are tuned to focus the beam at the DLW location. The beam size at the center of the structure is measured to be $\sigma_\perp^* = 102 \pm 5$ μm for a bunch charge of $Q = 1.1 \pm 0.05$ nC; the measurement was made by placing a Ce:YAG screen below the DLW holder on an actuator. Two DLW structures (DLW1 and 2) with different dimensions were available to our experiment; see Table I. Both structures consist of a hollow fused-silica tube
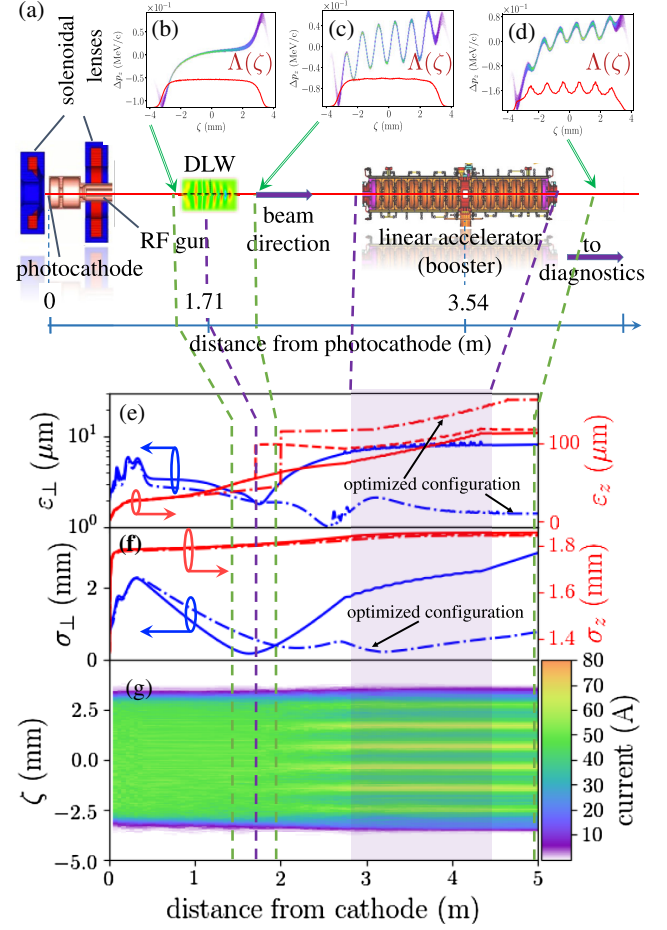

FIG. 1. Overview of the passive ballistic-bunching experiment implemented at the PITZ facility. (a) Simulated evolutions of the longitudinal-phase-space density distribution (ζ, δ) at the different stages of the bunching process (b)–(d) with associated current profile [$\Lambda(\zeta)$], evolution of the transverse and longitudinal emittances (e) and rms beam size (f) along the accelerator beamline with (dashed trace) and without (solid trace) DLW2 present, and development of the bunch current profile [$I(\zeta)$] along the beam line (g). The nominal parameters for these simulations are listed in Table I for the case of DLW2. Values $\zeta > 0$ correspond to the head of the bunch. Note that in plots (e) and (f) the dashed and solid traces overlap for the transverse parameters. For the "optimized configuration" an additional solenoid was located at $z = 2.7$ m.

with its outer surface metalized. Downstream of the linac, a suite of beam diagnostics enables the measurement of the LPS distribution and beam parameters; see Table I.

In order to gain further insights on the experiment, we performed supporting numerical simulations of the beam dynamics using the program ASTRA [26]. The software solves the equation of motion for electron macroparticles representing the bunch in the presence of externally applied user-defined electromagnetic fields and the beam's self-field (space charge). The electron-beam dynamics in the DLW is modeled using a Green's function approach

TABLE I.   Settings of accelerator parameters relevant to the experiment. The listed value for the phases are offset with respect to the maximum momentum gain phase.

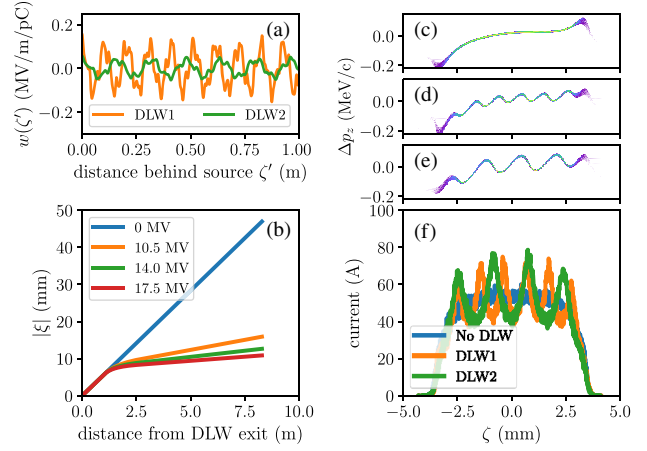| Parameter	Symbol	Nominal	Range	Unit
Laser launch phase	ϕ_l	0	$\cdots$	deg
Laser spot radius	r_l	2	$\cdots$	mm
Laser pulse duration	L_t	13	[10, 20]	ps
RF gun peak field	E_0	60	[45, 60]	MV/m
Linac phase	φ_b	0	[−20, +10]	deg
Linac voltage	V_b	14	[10, 18]	MV
Bunch charge	Q	1.1	[0.020, 2]	nC
Beam momentum	$\langle p \rangle$	21.8	[16, 22]	MeV/c
DLW permittivity	ε_r	4.41	$\cdots$	$\cdots$
DLW1 inner radius	a_1	450 ± 50	$\cdots$	μm
DLW1 outer radius	b_1	550 ± 50	$\cdots$	μm
DLW1 length	l_1	50.0 ± 0.1	$\cdots$	mm
DLW2 inner radius	a_2	750 ± 50	$\cdots$	μm
DLW2 outer radius	b_2	900 ± 50	$\cdots$	μm
DLW2 length	l_2	80.0 ± 0.1	$\cdots$	mm

FIG. 2.   Green's function for the two considered DLW structures. (a) Simulated evolution of the compression factor $|\xi|(z - z_c)$ along the beam line downstream of the DLW location for different booster-linac accelerating voltage V_b (b) and final LPS distribution obtained for the nominal accelerator settings for the cases without DLW (c) and with DLW1 (d) or DLW2 (e) inserted along with corresponding current profiles (f).

detailed in Ref. [27]. The Green's function is computed following the algorithm presented in Ref. [28]. This model was used to produce the sequence of LPS snapshots displayed in Figs. 1(b)–1(d) and was benchmarked against a first-principles electrodynamics simulation performed with the software, ECHO [29]. The corresponding beam parameters [root-mean square (rms) sizes, emittances $\varepsilon_u \equiv 1/(mc)[\langle u^2 \rangle \langle p_u^2 \rangle - \langle u p_u \rangle^2]^{1/2}$ along the transverse ($u = \perp$) and longitudinal ($u = z$) degrees of freedom] are displayed in Figs. 1(e)–1(f)—the beam is cylindrical symmetric. Additionally, the simulation allows for a numerical evaluation of the longitudinal dispersion taking into account the acceleration $\xi(z) = \int_{z_c}^{z} dz'/\gamma_f^2(z')$ downstream of the DLW (here $z > z_c = 1.71$ m is the position along the beam line). It is especially found that ξ increases slowly downstream of the linac thereby effectively "freezing" the current profile. The latter effect is also supported by the evolution of the bunch current profile along the beam line; see Fig. 1(g). For completeness the Green's functions employed are shown in Fig. 2(a). The evolution of ξ along the beam line appears in Fig. 2(b) together with the final LPS and current distribution obtained for the various cases (no DLW, DLW1, and DLW2 inserted); see Figs. 2(c)–2(e). Additionally, the simulations were performed with and without considering the effect of the DLW and confirmed the minimal impact of the DLW on the transverse phase-space parameters as quantified by the negligible change on the transverse-emittance evolution; see Fig. 1(f). The large transverse emittance excursions along the beam line are due to the PITZ nominal beam line configuration: the addition of a second solenoidal lens between the DLW and booster would allow a better emittance control to attain a final value of 1.4 μm as shown the Figs 1(e), 1(f) (dash-dotted lines). Finally, while the longitudinal emittance is significantly

increased at the DLW location due to the imparted energy modulation, the final longitudinal emittance downstream of the linac is only increased by < 5% when the DLW is included compared to the case without a DLW; see Fig. 1(e).

The backbone diagnostics is an S-band ($f = 2.997$ GHz) transverse deflecting structure (TDS) used to streak the beam [30]. The TDS ($z = 10.985$ m), vertically streaks the beam so that the vertical beam distribution measured on a Ce:YAG screen located ~ 1.3 m from the TDS center is representative of the temporal bunch distribution; the vertical coordinate of an electron is related to its axial position via $y \simeq S \zeta$ where the shearing parameter S [31] is inferred from a beam-based calibration procedure. It should be noted that in the present experiment the temporal resolution of the streaking was limited to ~ 0.5 ps.

The operating parameters of the rf gun and linac were tuned to optimize the bunching process. Ultimately a $\sim$ twofold peak-current enhancement was observed. The measured streaked density distributions appear in Figs. 3(a)–3(c) for the three cases under investigations (no DLW structure versus DLW1 or DLW2 structures inserted). The associated current profiles are displayed in Fig. 3(d) and indicate that peak currents close to ~ 90 A are attained when the beam is propagated through a DLW. The observations are in qualitative agreement with the simulated current profiles; see Fig 2(e): similar current-enhancement factors are measured when the beam passes through one of the structures. The disagreement in absolute peak current is attributed to the lack of precise knowledge of the initial photocathode drive-laser temporal profile along with the possible contributions from other wakefield sources which could change the overall correlation along the bunch and correspondingly affect the
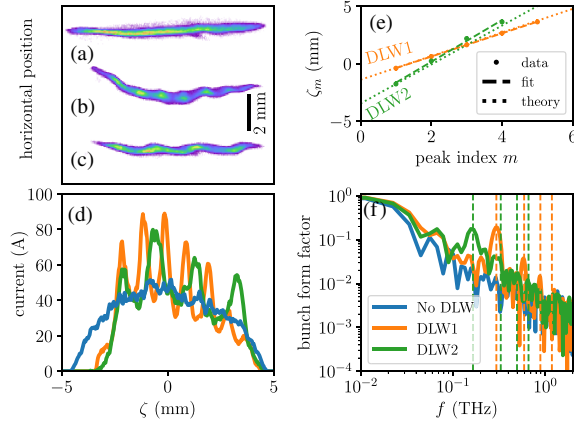
FIG. 3. Measured $Q(\zeta, x)$ charge-density distribution without DLW (a) and with DLW1 (b) or DLW2 (c) inserted, along with associated current profiles $I(\zeta)$ (d). Locations of local maxima for the current profiles measured with the DLW structures inserted (e) and associated bunch form factors (f).

peak currents. To further quantify the origin of the observed modulation, the locations of the peaks $\zeta_m = m\lambda_1 + \zeta_{\mathrm{off}}$ (where m is an integer and ζ_{off} an arbitrary offset) are measured thereby providing the wavelength of the modulation λ_1. The results of linear regressions give $\lambda_1^{\mathrm{DLW1}} = 1.01 \pm 0.10$ and $\lambda_1^{\mathrm{DLW2}} = 1.81 \pm 0.10$ mm, in good agreement with the expected fundamental-mode wavelengths of $\lambda_1^{\mathrm{DLW1}} = 1.02 \pm 0.16$ and $\lambda_1^{\mathrm{DLW2}} = 1.58 \pm 0.17$ mm, respectively; see Fig. 3(e). These values are obtained by directly solving the dispersion equation for the considered DLW with computed error bars accounting for the fabrication uncertainties listed in Table I.

Finally, the individual peak durations can be further quantified by computing the bunch form factor (BFF) $b(f) \propto |\int_{-\infty}^{+\infty} dt I(\zeta/c) e^{-2\pi f \zeta/c}|^2$ of the current profile in the frequency (f) domain via a fast Fourier transform (FFT) algorithm; see Fig. 3(f). When one of the DLWs is inserted, the BFF displays the expected spectral enhancement at $f_1 \simeq c/\lambda_1$ and at some of the harmonics frequencies $f_n = nf_1$ (where n is an integer). DLW1 especially yields a spectral enhancement at the 3rd harmonic ($f_3 \simeq 1$ THz) confirming the current modulations have a duration $\tau < 1/f_3 \simeq 1$ ps, an upper value set by the resolution of the TDS-based technique.

An important capability of the experimental configuration is the longitudinal-phase-space control enabled by the linac located downstream of the DLW. Operating the linac off-crest provides a knob to introduce a correlation between the time and energy coordinates. During acceleration through the booster linac the fractional momentum spread evolves as $\delta_f \to \delta_b = (1/\gamma_b)\{\gamma_f \delta_f + \Gamma_b[\cos(k_b\zeta_f + \varphi_b) - \cos(\varphi_b)]\} \simeq (\gamma_f/\gamma_b)\delta_f + \mathcal{C}\zeta_f$ where the right-hand side approximation stems from the assumption $k_b\zeta \ll 1$, and $\gamma_b \equiv \gamma_f + \Gamma_b\cos(\varphi_b)$ is the final Lorentz factor downstream of the linac with $\Gamma_b \equiv eV_b/(mc^2)$, where V_b is the
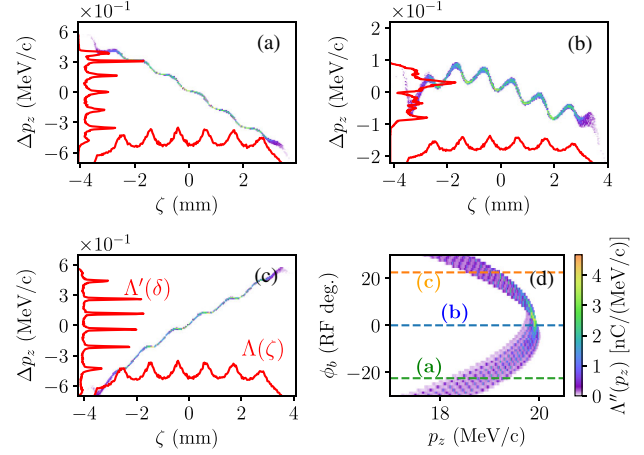

FIG. 4. Simulated evolution of the LPS for booster linac injection phases $\varphi_b = -22.5°$ (a), $0°$ (b), and $+22.5°$ (c). The traces correspond to the peak-normalized charge distribution as a function of longitudinal (energy) $\Lambda(\zeta)$ [$\Lambda'(\delta)$] coordinate. Evolution of the charge distribution $\Lambda''(p_z)$ for different injection phases φ_b (d) with labeled lines referring to phase settings associated with plots (a),(b), and (c). The simulations are performed with DLW2 (similar results are obtained with DLW1 albeit with a different modulation period).

booster-linac accelerating voltage. The booster wave-vector amplitude is $k_b = 27.3$ m^{-1}. Therefore off-crest ($\varphi_b \neq 0$) operation imposes a linear correlation $\mathcal{C} \equiv -k_b\Gamma_b/\gamma_b \sin\varphi_b$ within the LPS.

The introduced LPS correlation can be taken advantage of to control, e.g., the energy of each microbunch within the beam as demonstrated via numerical simulations in Fig. 4. Given that the bunch is relativistic, the longitudinal motion is unaffected by the phase of the booster and the temporal modulation is solely set by the DLW parameters. To demonstrate this LPS-control feature, we further propagated the vertically streaked beam to a horizontally energy-dispersive beam line and measured the beam distribution on a downstream Ce:YAG screen ($z = 20.885$ m). Under proper optimization, the coordinates of an electron are given by $y = \mathcal{S}'\zeta$ (where $\mathcal{S}' \neq \mathcal{S}$) and $x = \eta\delta$ (where $\eta \simeq 0.9$ m is the dispersion function at the observation point) thereby enabling a direct measurement of the LPS density distribution. Figure 5(a) displays snapshots of the LPS-density distribution measured for the three configurations and for four sets of the booster-cavity phase and qualitatively illustrates the control over the $\zeta - \delta$ correlation along the bunch. The LPS measurement is limited and we therefore measure the location of the LPS peaks value to infer the longitudinal $\Delta\zeta$ and energy $\Delta\delta$ separations between the peaks; see Figs. 5(b), 5(c). The data are in agreement with the simulations and confirm that tuning the phase φ_b controls the energy separation between the microbunches while not affecting their longitudinal separation resulting in a tunable correlation between the microbunches. Consequently, the control enabled by ϕ_b together with the
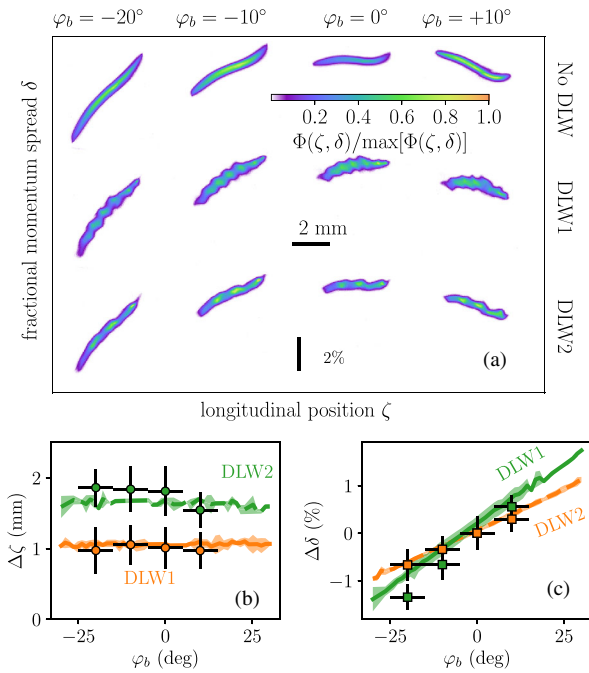
FIG. 5. Mosaic image of measured LPS-distribution snapshots (a) for different settings of the booster linac injection phases φ_b (columns) corresponding to the three cases of DLW operation (rows). Comparison of the simulated (traces) and measured (symbols) modulation period along the longitudinal $\Delta\zeta$ (b) and fractional energy $\Delta\delta$ (c) coordinates. The shaded areas reflect uncertainties in the simulated values.

ability to insert different structures provides a method to tailor the microbunch energy and longitudinal spacings. Such a versatile manipulation technique could have applications to multicolor free-electron lasers [32] or could be used in single-shot time-resolved UED.

In summary, we have demonstrated the basic features of a simple method to passively form a modulated beam by exploiting the beam-induced electromagnetic wakefields produced in a dielectric-lined waveguide; we note the concept could work with other high-impedance mediums also, e.g., corrugated structures or plasmas. Although our observation leads to a modest peak current enhancement of a factor ~2, our simulations indicate the concept could be scaled to kA-class peak currents [7]. Additionally, with longer DLW lengths and optics considerations, bunching may occur within the structure and yield the emission of coherent enhanced Čerenkov radiation akin to a single-pass FEL process [33]; for our experimental conditions, the gain length of the process is estimated to be $\ell \simeq 1.5$ cm using a 1D model. The simplicity and compactness of the demonstrated technique together with its versatility (it can be coupled to any electron-emission process) are appealing features that should motivate its implementation in compact electron sources being developed in support to fundamental research or various societal applications.

*francois.lemery@gmail.com

[1] R. J. England, J. B. Rosenzweig, and G. Travish, Phys. Rev. Lett. **100**, 214802 (2008).

[2] P. Muggli, V. Yakimenko, M. Babzien, E. Kallos, and K. P. Kusche, Phys. Rev. Lett. **101**, 054801 (2008).

[3] Y.-E Sun, P. Piot, A. Johnson, A. H. Lumpkin, T. J. Maxwell, J. Ruan, and R. Thurman-Keup, Phys. Rev. Lett. **105**, 234801 (2010).

[4] P. Piot, C. Behrens, C. Gerth, M. Dohlus, F. Lemery, D. Mihalcea, P. Stoltz, and M. Vogt, Phys. Rev. Lett. **108**, 034801 (2012).

[5] G. Ha *et al.*, Phys. Rev. Lett. **118**, 104801 (2017).

[6] S. Antipov, M. Babzien, C. Jing, M. Fedurin, W. Gai, A. Kanareykin, K. Kusche, V. Yakimenko, and A. Zholents, Phys. Rev. Lett. **111**, 134802 (2013).

[7] F. Lemery and P. Piot, Phys. Rev. ST Accel. Beams **17**, 112804 (2014).

[8] G. Andonian, S. Barber, F. H. O'Shea, M. Fedurin, K. Kusche, C. Swinson, and J. B. Rosenzweig, Phys. Rev. Lett. **118**, 054802 (2017).

[9] C. Lu, T. Jiang, S. Liu, R. Wang, L. Zhao, P. Zhu, D. Xiang, and J. Zhang, Phys. Rev. Lett. **120**, 044801 (2018).

[10] B. E. Carlsten and S. J. Russell, Phys. Rev. E **53**, R2072 (1996).

[11] B. Johnson and J. Walsh, Nucl. Instrum. Methods Phys. Res., Sect. A **237**, 239 (1985).

[12] E. P. Garate, J. Walsh, C. Shaughnessy, B. Johnson, and S. Moustaizis, Nucl. Instrum. Methods Phys. Res., Sect. A **259**, 125 (1987).

[13] F. Ciocci, A. Doria, G. P. Gallerano, I. Giabbai, M. F. Kimmitt, G. Messina, A. Renieri, and J. E. Walsh, Phys. Rev. Lett. **66**, 699 (1991); Z. Phys. **95**, 752 (1935).

[14] R. Talman, Phys. Rev. Lett. **56**, 1429 (1986).

[15] P. Piot, in *Proceedings of FEL15, Daejeon, Korea*, edited by H. S. Kang, D.-E. Kim, and V. RW. Schaa (2015) p. 274, ISBN: 978-3-95450-134-2.

[16] A. Gover, Phys. Rev. ST Accel. Beams **8**, 030701 (2005).

[17] E. A. Schneidmiller, T. Tschentscher, K. Tiedtke, M. V. Yurkov, M. Krasilnikov, and F. Stephan, Proc. SPIE Int. Soc. Opt. Eng. **8778**, 877811 (2013).

[18] A. H. Zewail and J. M. Thomas, *4D Electron Microscopy: Imaging in Space and Time* (Imperial College Press, London, 2010).

[19] R. K. Li, P. Musumeci, H. A. Bender, N. S. Wilcox, and M. Wu, J. Appl. Phys. **110**, 074512 (2011).

[20] S. P. Weathersby *et al.*, Rev. Sci. Instrum. **86**, 073702 (2015).

[21] J. G. Power, M. E. Conde, W. Gai, R. Konecny, P. Schoessow, and A. D. Kanareykin, Phys. Rev. ST Accel. Beams **3**, 101302 (2000).

[22] H. G. Dawson, Proc. London Math. Soc. **s1-29**, 519 (1897).

[23] M. Krasilnikov *et al.*, Phys. Rev. ST Accel. Beams **15**, 100701 (2012).

[24] V. Paramonov *et al.*, *Proceedings of LINAC2010, Japan MOP81*, edited by M. Ikegami, V. Schaa, and H. Sako (2010), p. 241, ISBN: 9783954500291.

[25] I. Will and G. Klemz, Opt. Express **16**, 14922 (2008).

[26] K. Flöttmann, ASTRA: A space charge algorithm, http://www.desy.de/~mpyflo/.

[27] M. Dohlus, K. Flöttmann, and C. Henning, arXiv:1201.5270.

[28] M. Rosing and W. Gai, Phys. Rev. D **42**, 1829 (1990).

[29] I. Zagorodnov, *Proceedings of NAPAC16, Chicago, IL, USA*, edited by M. Power, V. Shiltsev, V. Schaa, and M. White (2016), p. 642, ISBN: 978-3-95450-180-9.

[30] E. N. Volobuev, A. A. Zavadtsev, D. A. Zavadtsev, L. V. Kravchuk, V. V. Paramonov, M. V. Lalayan, A. J. Smirnov, N. P. Sobenin, and D. V. Churanov, J. Phys. Conf. Ser. **747**, 012083 (2016).

[31] K. Floettmann and V. V. Paramonov, Phys. Rev. ST Accel. Beams **17**, 024001 (2014).

[32] E. Roussel, E. Ferrari, E. Allaria, G. Penco, S. Di Mitri, M. Veronese, M. Danailov, D. Gauthier, and L. Giannessi, Phys. Rev. Lett. **115**, 214801 (2015).

[33] G. Stupakov, Phys. Rev. ST Accel. Beams **18**, 030709 (2015).